blood®
Regular Article

IMMUNOBIOLOGY AND IMMUNOTHERAPY

CXCR4 signaling controls dendritic cell location and activation at steady state and in inflammation

Carmen Gallego,[1,*] Mathias Vétillard,[1,*] Joseph Calmette,[1,†] Mélanie Roriz,[1,†] Viviana Marin-Esteban,[1] Maximilien Evrard,[2] Marie-Laure Aknin,[3] Nicolas Pionnier,[1] Manon Lefrançois,[1] Françoise Mercier-Nomé,[3] Yves Bertrand,[4] Felipe Suarez,[5] Jean Donadieu,[6,7] Lai Guan Ng,[2] Karl Balabanian,[1,8] Françoise Bachelerie,[1] and Géraldine Schlecht-Louf[1]

[1]Université Paris-Saclay, INSERM, Inflammation, Microbiome and Immunosurveillance, Clamart, France; [2]Singapore Immunology Network (SIgN), Agency for Science, Technology and Research (A*STAR), Biopolis, Singapore—School of Biological Sciences, Nanyang Technological University, Singapore; [3]Ingénierie et Plateformes au Service de l'Innovation Thérapeutique (IPSIT) Structure Fédérative de Recherche–Unité Mixte de Service (SFR-UMS), Chatenay-Malabry, France; [4]Institut d'Hématologie et Oncologie Pédiatrique–Hématologie et Immunologie Pédiatrique, Hôpitaux Civils de Lyon, Lyon, France; [5]Laboratory of Molecular Mechanisms of Hematological Disorders and Therapeutic Implications, Imagine Paris, Paris, France; [6]Service d'Hématologie–Immuno-Oncologie Pédiatrique Registre des Neutropénies Assistance Publique–Hôpitaux de Paris (AP-HP), Hôpital d'Enfants Armand Trousseau, Paris, France; [7]Sorbonne Université, INSERM, Centre de Recherche Saint-Antoine, Centre de Recherche Saint-Antoine (CRSA), Paris, France; and [8]Université de Paris, Institut de Recherche Saint-Louis, EMiLy, INSERM, Paris, France

KEY POINTS

- **Natural CXCR4 mutants show subset-specific effects of CXCR4 signaling on the dynamics of DC migration in vivo.**
- **Proper CXCR4 signaling directs efficient skin DC migration to lymph nodes, thus controlling their activation state.**

Dendritic cells (DCs) encompass several cell subsets that collaborate to initiate and regulate immune responses. Proper DC localization determines their function and requires the tightly controlled action of chemokine receptors. All DC subsets express CXCR4, but the genuine contribution of this receptor to their biology has been overlooked. We addressed this question using natural CXCR4 mutants resistant to CXCL12-induced desensitization and harboring a gain of function that cause the warts, hypogammaglobulinemia, infections, and myelokathexis (WHIM) syndrome (WS), a rare immunodeficiency associated with high susceptibility to the pathogenesis of human papillomavirus (HPV). We report a reduction in the number of circulating plasmacytoid DCs (pDCs) in WHIM patients, whereas that of conventional DCs is preserved. This pattern was reproduced in an original mouse model of WS, enabling us to show that the circulating pDC defect can be corrected upon CXCR4 blockade and that pDC differentiation and function are preserved, despite CXCR4 dysfunction. We further identified proper CXCR4 signaling as a critical checkpoint for Langerhans cell and DC migration from the skin to lymph nodes, with corollary alterations of their activation state and tissue inflammation in a model of HPV-induced dysplasia. Beyond providing new hypotheses to explain the susceptibility of WHIM patients to HPV pathogenesis, this study shows that proper CXCR4 signaling establishes a migration threshold that controls DC egress from CXCL12-containing environments and highlights the critical and subset-specific contribution of CXCR4 signal termination to DC biology. (*Blood*. 2021;137(20):2770-2784)

Introduction

Dendritic cells (DCs) are a heterogeneous group of innate cells that control tolerance and immunity.[1] They encompass plasmacytoid DC (pDC) and type 1 and 2 conventional DCs (cDCs), identified in humans and mice based on ontogenic, phenotypic, and functional criteria.[2-5] DCs originate in the bone marrow (BM), either as fully differentiated pDCs, arising from both lymphoid and myeloid progenitors,[5-7] or as myeloid-derived cDC precursors (pre-cDCs), which complete their differentiation in peripheral tissues or lymphoid organs (LOs).[3,8] Langerhans cells (LCs)[9] are an additional DC-like subset that collaborate with bona fide DCs to shape immune responses.

pDCs are circulating sentinels[10] that promote antiviral immunity by type I interferon (IFN) secretion. In peripheral tissues, cDCs and LCs collect antigens before trafficking to secondary LOs (SLOs) as migratory DCs (migDCs) and migratory LCs, where they reach the T-cell zone to prime adaptive immune responses together with resident DCs (resDCs) and pDCs.[11,12] The appropriate pDC and pre-cDC distribution throughout the tissues, as well as cDC and LC patrolling and directed migration to lymph nodes (LNs) warrant DC function.[13,14] Although CCR7 and its ligands, CCL19 and CCL21, form the main chemokine (CK) receptor-CK axis that controls DC migration to and within SLOs,[12,15-17] additional CKs and their receptors may regulate their location,[10,12] including CXCR4 and its sole CK ligand, CXCL12.[11,12,18-20]

CXCR4 is a broadly expressed Gαi protein-coupled receptor,[11] including in DCs, of which activation by CXCL12 is essential for myelopoiesis.[21] CXCL12[22] is highly produced by dermal fibroblasts,

BM-derived mesenchymal cells, endothelial cells, and DCs.[23-28] Although studies based on knock-out models and pharmacological blockade have revealed a role for CXCR4 in pDC differentiation,[29,30] pDC and pre-cDC retention in the BM,[31,32] and pDC,[33] LC,[34] and cDC migration,[11,26] the true contribution of its signaling in DC subset homeostasis and function remains elusive. This can be addressed using natural CXCR4 mutants that cause the warts, hypogammaglobulinemia, infections, and myelokathexis (WHIM) syndrome (WS). This rare immunodeficiency mainly results from heterozygous *CXCR4* mutations, leading to CXCR4 carboxyl-terminal domain truncation and subsequent gain-of-function and impaired desensitization (ie, dysfunction).[25,35,36] WS manifests by panleukopenia[37,38] and profuse intractable human papillomavirus (HPV)-induced warts that often evolve toward carcinoma.[25,39-43] In this context, Tassone et al reported quantitative circulating DC defects in WHIM patients.[44] However, the genuine impact of CXCR4 dysfunction on DC-subset differentiation, migration, and function, and thus the role of proper CXCL12/CXCR4 signaling in DC biology, have not been yet investigated.

Here, we used WS-associated CXCR4 mutations to address this issue. Our results in WHIM patients challenge those of a previous report,[44] as we show quantitative defects for circulating pDC but not cDC subsets. They were confirmed in *Cxcr4*$^{+/1013}$ knock-in mice that replicate WS-associated immune-hematological defects.[25,45] In these mice, we show that pDC differentiation and function are preserved and that the pDC peripheral defect can be explained by their entrapment in the BM. Although LCs and dermal DCs were quantitatively preserved in *Cxcr4*$^{+/1013}$ mice, their migration to LNs was markedly reduced, both at steady state and in a model of HPV-induced dysplasia. In addition, *Cxcr4*$^{+/1013}$ migDCs (migDC$^{+/1013}$) recovered from LNs were more activated than their wild-type (WT) counterparts, likely because of the selective egress of only the most activated skin DC$^{+/1013}$. Overall, our results unravel the specific importance of proper CXCR4 signaling in DC-subset biology and its profound impact on immune homeostasis.

Methods

Human samples

WHIM patients were recruited from the French Severe Chronic Neutropenia Registry (J.D.), approved by the "Commission Nationale de l'Informatique et des Libertés." The patients provided written informed consent for genetic testing and inclusion in the registry. The patients and their genetic mutations (supplemental Table 1, available on the *Blood* Web site) have been described.[41,46]

Blood samples were collected in lithium-heparin–coated tubes. For each patient sample, a sample from a healthy donor was collected at the same time and place for parallel analysis.

Mice

Cxcr4$^{+/1013}$ mice harboring the WS-associated *CXCR4*^{1013} mutation on the C57BL/6J and FVB/N genetic backgrounds were previously described.[45,47] K14-HPV16 (HPV) transgenic mice expressing HPV early genes under the control of the keratin 14 promoter[48,49] were obtained from the National Cancer Institute mouse repository. K14-HPV16 *Cxcr4*$^{+/1013}$ (HPV+/1013) mice were generated by crossing FVB/N *Cxcr4*$^{+/1013}$ mice with HPV mice.[47]

Except for parabiosis experiments, experimental procedures were conducted in the AnimEx animal facility (agreement no. B 92-023-01) in accordance with European Union legislation concerning the use of laboratory animals and approved by the Institutional Animal Care and Ethics Committee CEEA26 (Institut Gustave Roussy, France). Data were obtained from 7- to 14-week-old mice. *Cxcr4*$^{+/1013}$ and HPV+/1013 mice were compared with their littermate *Cxcr4*$^{+/+}$ and HPV controls.

Parabiosis experiments were performed in the Biological Resource Centre of A*STAR, under the authorization of the Institutional Animal Care and Use Committee of the Biological Resource Centre, in accordance with the guidelines of the Agri-Food and Veterinary Authority and the National Advisory Committee for Laboratory Animal Research of Singapore.

Parabiosis

Female CD45.2 *Cxcr4*$^{+/1013}$ and CD45.1 control mice were anesthetized using 2.5% avertin (15 mL/kg) and surgically joined, as previously described.[50] Mice then received Baytril and buprenorphine subcutaneously (0.05-2 mg/kg and 5-20 mg/kg, respectively). After 8 weeks, blood was recovered from each parabiont. Spleens and BM were harvested after perfusion. The blood volume present in each individual mouse was calculated as follows: blood volume (mL) = 0.0715 × body weight (g).[51] Spleen/blood ratios were calculated as the number of cells in nonhost organ divided by the number of cells in nonhost blood, as previously described.[50]

In vivo mobilization

Mice were injected intraperitoneally with AMD3100 (Sigma-Aldrich) or phosphate-buffered saline. Two hours later, blood was collected for flow cytometry.

FITC painting assays

A solution of fluorescein isothiocyanate (FITC) (1 mg/mL in acetone; Merck) was mixed (v/v) with dibutyl phthalate and 100 μL applied to the abdomen. Mice were euthanized 24 hours later and migration of skin DCs to draining lymph nodes (SDLNs) was assessed by flow cytometry. For CXCR4 blockade, AMD3100 (0.8 mg/kg) was injected intraperitoneally at t = 0 and t = 6 hours. FITC application was performed 1 hour after the first AMD3100 injection.

Mouse samples

Skin cell isolation, performed as previously described,[52] as well as blood, spleen, LN, and BM cell preparation are detailed in supplemental Methods. Splenic pDCs, as well as Flt3-L-derived, cDC1-like, and cDC2-like BMDCs were obtained as previously described.[53-55]

Epidermal sheets

Epidermal sheets were prepared as previously described.[52] Details are provided in supplemental Methods.

DC activation

For in vivo stimulation, mice were injected intraperitoneally with 20 μg CpG-ODN 2216 (Invivogen) in a complex with 30 μg DOTAP liposome (Sigma-Aldrich), as previously described.[56] Control mice received DOTAP only.

In vitro activation is detailed in supplemental Methods.

Cytokine quantification

The IFN-α concentrations in cell supernatants and CCL2, CCL4, and CXCL10 concentrations in mouse serum were quantified using a Mouse IFN α Platinum enzyme-linked immunosorbent

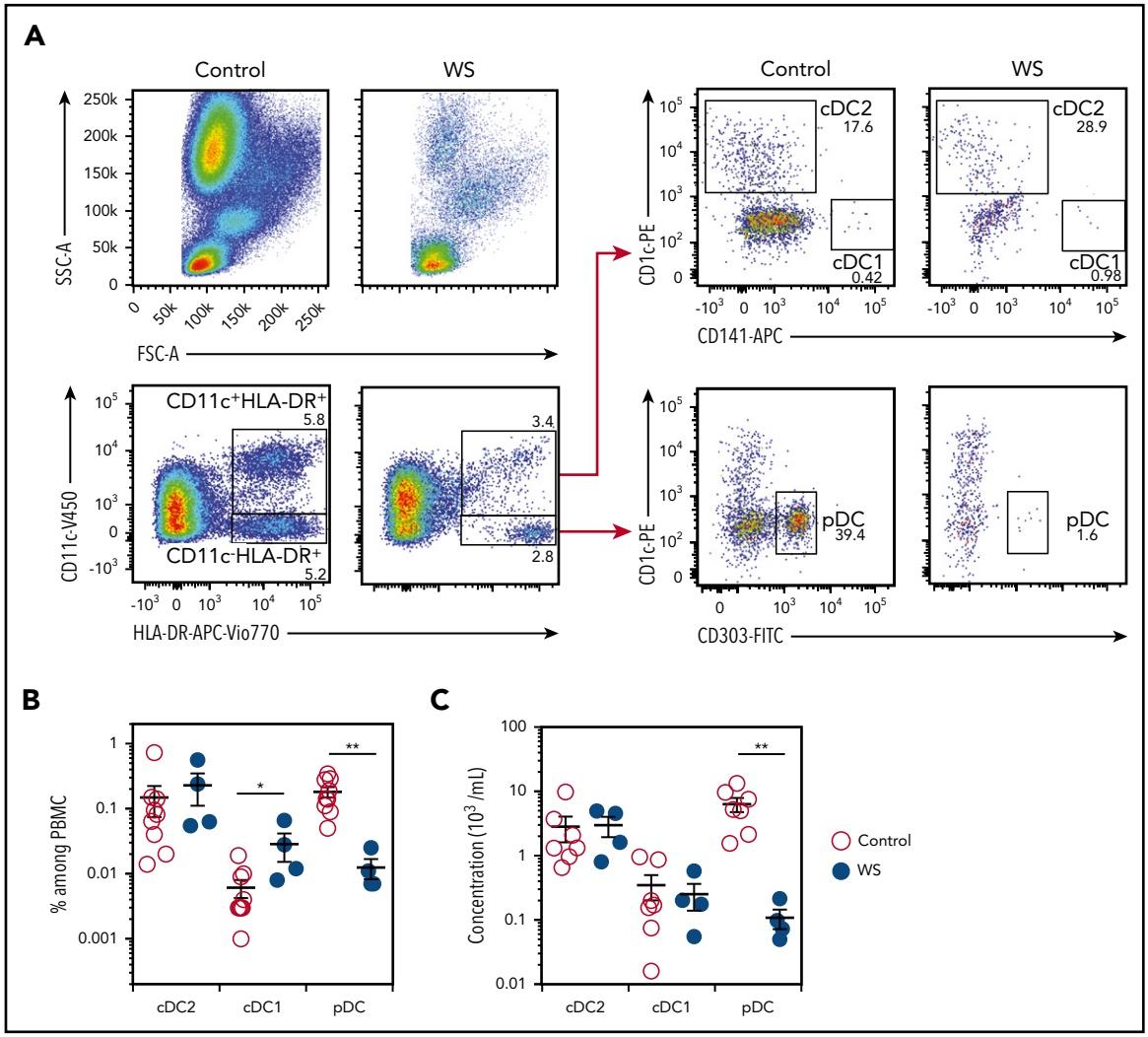

Figure 1. WHIM patients harbor quantitative defects in pDCs. (A) Blood DC subsets were analyzed in WHIM patients and healthy donors. Representative pseudo-color dot plots obtained for the same volume of blood from 1 healthy control (control) and 1 WHIM patient (WS) carrying the heterozygous *CXCR4*$^{+/1013}$ mutation are shown. cDC2 was defined as CD11c^{+}HLA-DR^{+}CD1c^{+} cells, cDC1 as CD11c^{+}HLA-DR^{+}CD141^{+} cells, and pDCs as CD11c^{-}HLA-DR^{+}CD303^{+} cells. Percentages among parent cells are indicated. (B-C) The frequency of DC subsets among peripheral blood mononuclear cells (B) and their concentrations (C) were measured for healthy controls (control) and WHIM patients (WS). Each point represents an individual and lines indicate the mean ± standard error of the mean (SEM). n = 9 Controls and n = 4 WS (B); n = 7 controls and n = 4 WS (C). Statistical analysis was performed using the 2-tailed, unpaired Mann-Whitney test. *$P < .05$, **$P < .01$.

assay (eBioscience) and U-PLEX Chemokine Combo Mouse Kit (Meso Scale Discovery), respectively.

Flow cytometry

Flow cytometry was performed as described in supplemental Methods.

Histology

Histology was performed as described in supplemental Methods.

Statistics

Statistical analyses were performed using Prism software (GraphPad). The 2-tailed Mann-Whitney test and paired *t* test were used to compare unpaired and paired data, respectively.

Results

WHIM patients display quantitative defects in circulating pDCs but not cDCs

We analyzed cDC1, cDC2, and pDC subsets in the blood of 4 previously described WHIM patients and 9 healthy controls. Patients were panleukopenic, as expected (Figure 1A).[41] Blood pDCs counts and frequencies were reduced (Figure 1B-C), as previously reported.[44] However, cDC1 and cDC2 frequencies were slightly higher and normal, respectively. These DC subsets showed no significant quantitative defects (Figure 1B-C), in contrast to the reduced percentages and counts reported by Tassone et al for the entire myeloid DC subset.[44] Thus, WS-associated CXCR4 mutations were associated with a quantitative defect of circulating pDC but not cDC subsets in the blood of the 4 analyzed patients.

Cxcr4$^{+/1013}$ mice reproduce WS-associated DC-subset alterations

We next analyzed DC subsets in *Cxcr4*$^{+/1013}$ mice, which harbor the WS-associated *CXCR4*^{1013} gain-of-function mutation[25] and model the panleukopenia reported in patients.[45] *Cxcr4*$^{+/1013}$ mice showed reduced splenic pDC frequency and cellularity (Figure 2A-C) and reduced splenocyte numbers (supplemental Figure 1A).[45] In contrast, the frequency of splenic *Cxcr4*$^{+/1013}$ cDCs (cDC$^{+/1013}$) was significantly higher, resulting in preservation of their number

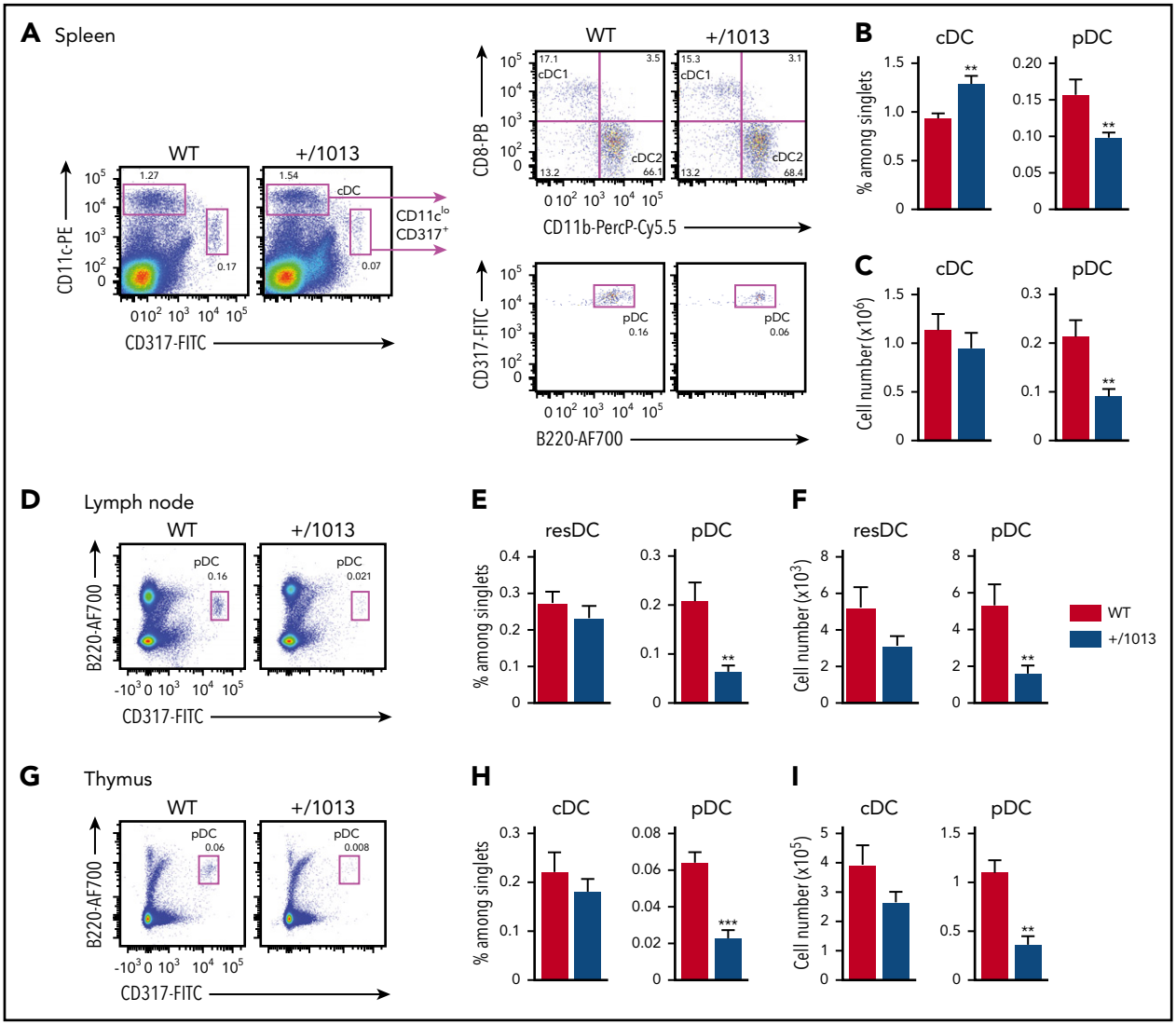

Figure 2. *Cxcr4*$^{+/1013}$ mice show a reduced pDC pool in the spleen, LNs, and thymus. (A) Representative dot plots show the gating strategy for cDC1 (CD11c^{hi}CD317^{-}CD11b^{-}CD8^{+}), cDC2 (CD11c^{hi}CD317^{-}CD11b^{+}CD8^{-}), and pDC (CD11c^{lo}CD317^{+}B220^{+}) identification in the spleens from *Cxcr4*$^{+/1013}$ (+/1013) and littermate *Cxcr4*$^{+/+}$ (WT) mice. The percentages of cDCs, CD11c^{lo}CD317^{+} cells, and pDCs among singlets and cDC1 and cDC2 among DCs are indicated. (B-C) Spleen cDCs and pDCs frequencies (B) and numbers (C) were determined by flow cytometry (n = 17 mice/group from 7 experiments). (D,G) Representative dot plots showing pDC gating in inguinal LNs (D) and the thymus (G) from +/1013 and WT mice. (E-F) Resident cDC (resDC, CD11c^{hi}CD317^{-}MHCII^{+}) and pDC (CD11c^{lo}CD317^{+}B220^{+}) frequencies (E) and numbers (F) in inguinal LNs from +/1013 and WT mice (n = 12-13 mice/group from 5 experiments). (H-I) cDC (CD11c^{hi}CD317^{-}) and pDC (CD11c^{lo}CD317^{+}B220^{+}) frequencies (H) and numbers (I) in thymuses from +/1013 and WT mice (n = 7-8 mice/group from 3 experiments). Bar graphs show the mean ± SEM. Mice had a C57BL/6J genetic background. Statistical analysis was performed using the 2-tailed, unpaired Mann-Whitney test. *$P < .05$, **$P < .01$, ***$P < .001$.

(Figure 2B-C), with no alteration in the relative proportion of cDC1s and cDC2s (supplemental Figure 1B). *Cxcr4*$^{+/1013}$ pDC (pDC$^{+/1013}$) expressed CD4, CD8α, CD9, and CCR9 similarly to control pDCs (pDC^{WT}), but included a subset of cells expressing low levels of SiglecH (supplemental Figure 2A), which may correspond to myeloid pDC-like cells.[7] pDC$^{+/1013}$ and cDC$^{+/1013}$ displayed enhanced chemotaxis toward CXCL12 in a transwell assay (supplemental Figure 2B), which was blocked by the CXCR4-specific antagonist AMD3100, with no alteration in CXCR4 cell-surface expression (supplemental Figure 2C). Further analyses in the LNs and thymus showed a lower number and frequency of pDC$^{+/1013}$ than pDC^{WT}, whereas LN resDC$^{+/1013}$ and thymic cDC$^{+/1013}$ frequencies were preserved (Figure 2D-I; supplemental Figure 1C-D). The blood pDC$^{+/1013}$ frequency and counts were also reduced and pre-cDC$^{+/1013}$ counts were diminished (supplemental Figure 3). Thus, *Cxcr4*$^{+/1013}$ mice display alterations in DC-subset distribution consistent with those observed in WHIM patients, including a marked quantitative deficit of pDCs.

CXCR4 dysfunction limits pDC egress from the BM while preserving their differentiation

We analyzed BM from *Cxcr4*$^{+/1013}$ and control mice to determine whether the reduced peripheral pDC$^{+/1013}$ number resulted from a production defect. The frequency of pDC$^{+/1013}$ was higher, although their total number remained similar to that of pDC^{WT} (Figure 3A-B) because of low BM cellularity (supplemental Figure 1E). Pre-cDC$^{+/1013}$ frequencies and numbers were preserved. Thus, WS-associated CXCR4 dysfunction does not hamper pDC nor pre-cDC differentiation. CXCR4 blockade upon injection of AMD3100 led to peripheral mobilization of pDC$^{+/1013}$

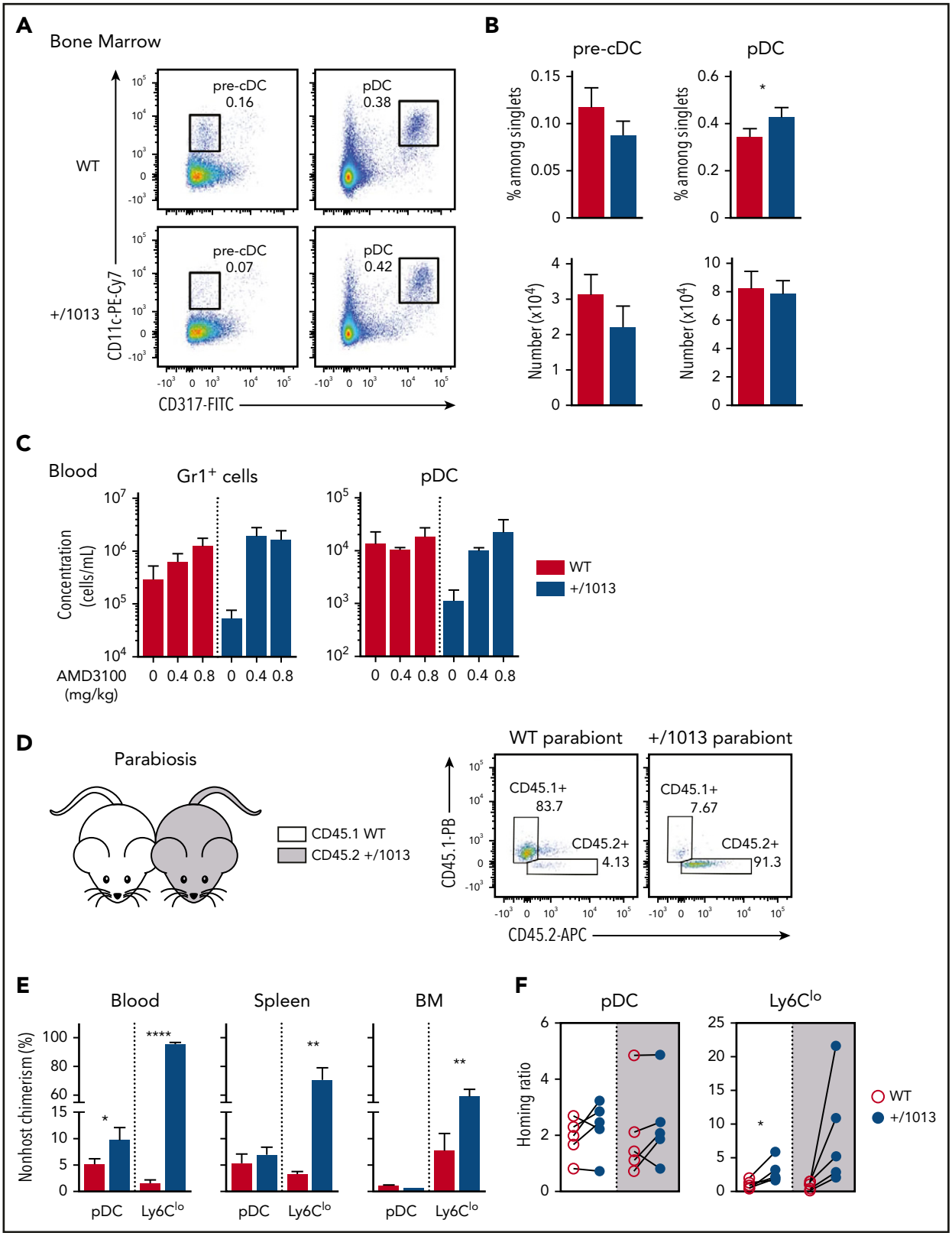

Figure 3. The peripheral pDC defect in *Cxcr4*$^{+/1013}$ mice results from impaired CXCR4-dependent pDC egress from BM. (A) Representative dot plots showing the gating strategy to identify pre-cDCs (CD11c^{lo}CD317^{-} gated on live CD4^{-}CD8^{-}B220^{-}CD11b^{+}MHC2$^{-/int}$ cells) and pDCs (CD11c^{lo}CD317^{+} among live B220^{+} cells) in the BM of +/1013 and WT mice. (B) Pre-cDC and pDC frequencies (top bar graphs) and numbers (bottom bar graphs) in the BM of +/1013 and WT mice (means ± SEM, n = 7-8 mice from 4 experiments for pre-cDC, n = 17 mice/group from 6 experiments for pDC frequency, n = 10-11 mice from 4 experiments for pDC number). (C) Numbers of blood pDCs and Gr1^{+} cells assessed 2 hours after intraperitoneal injection of AMD3100 or phosphate-buffered saline (mean ± SEM, n = 3 mice/group, 1 representative experiment of 2). (D-F) Parabiosis experiments were performed with CD45.1 *Cxcr4*$^{+/+}$ (WT, left parabiont) and CD45.2 *Cxcr4*$^{+/1013}$ (+/1013, right parabiont) mice. Blood, spleen, and BM were analyzed 8 weeks later. (D, right) Representative dot plots showing CD45.1 and CD45.2 expression in blood pDCs from WT and +/1013 parabionts. (E) Nonhost chimerism in the blood,

and normalization of their circulating counts (Figure 3C), consistent with these cells being trapped in the BM. Medullar pDC$^{+/1013}$ and pDC^{WT} expressed similar levels of CXCR4 (supplemental Figure 4A), ruling out pDC$^{+/1013}$ retention resulting from increased CXCR4 cell-membrane expression. Further analysis of Ki67 and cleaved caspase 3 expression (supplemental Figure 4B-C) support the conclusion that pDC$^{+/1013}$ divide less and are more prone to apoptosis than pDC^{WT}, likely because of their medullar retention.

We further investigated the contribution of CXCR4 to pDC trafficking and homing to and residency in LO by establishing parabiosis between CD45.2 *Cxcr4*$^{+/1013}$ and CD45.1 control mice (Figure 3D-F). Although nonhost chimerism was limited for blood pDCs (Figure 3E), in accordance with their short half-life in circulation,[57,58] it was twofold higher in *Cxcr4*$^{+/1013}$ parabionts than in WT ones. This difference likely reflects the reduced number of circulating pDC$^{+/1013}$ (Figure 3E). In contrast, such a relative increase of pDC^{WT} over pDC$^{+/1013}$ was observed neither in the BM nor spleens of *Cxcr4*$^{+/1013}$ parabionts, suggesting that CXCR4 dysfunction may affect pDC entry into these organs. We thus calculated spleen/blood ratios,[50] which allowed normalization for cell chimerism. These ratios were similar for pDC$^{+/1013}$ and pDC^{WT}, regardless of the spleen genetic background, suggesting similar entry and residency of these cells in this LO. This contrasted with nonclassical Ly6C^{lo} monocyte ratios (Figure 3F) whose trafficking was affected by CXCR4 dysfunction as reported.[50] Thus, the quantitative defects in peripheral pDC$^{+/1013}$ likely result from their reduced egress from the BM, as described for *Cxcr4*$^{+/1013}$ BM neutrophils,[45] confirming the reported role of CXCR4 in pDC egress from BM.[31] Meanwhile, pDC differentiation, entry, and residency in the spleen are preserved.

pDC$^{+/1013}$ display efficient innate functions

Most WHIM patients suffer from severe HPV-associated pathogenesis, suggesting impaired antiviral responses. We thus investigated the impact of CXCR4 dysfunction on pDC functions. pDC$^{+/1013}$ tended to produce less IFN-α than pDC^{WT} upon Toll-like receptor 9 (TLR9) engagement by CpG-ODN (Figure 4A, left). However, they also survived less in culture (Figure 4A, right) and were more prone to apoptosis than pDC^{WT} (Figure 4B). In addition, pDC-like BMDC$^{+/1013}$ and BMDC^{WT} produced similar levels of IFN-α upon TLR9 engagement (Figure 4C). Overall, these experiments suggest that pDC$^{+/1013}$ display preserved IFN-α responses.

We next tested the impact of CXCR4 dysfunction on the capacity of pDCs to initiate innate immune responses in a model of CpG-induced inflammation, in which pDCs are instrumental for myeloid cell recruitment to the peritoneum and natural killer (NK) cell activation.[56] Upon CpG-ODN injection, both *Cxcr4*$^{+/1013}$ mice and their controls showed increased cellularity and marked changes in the type of cells recovered from peritoneal lavages relative to vehicle (veh)-treated mice (Figure 4D-E). Although threefold fewer pDCs were present in the peritoneum of *Cxcr4*$^{+/1013}$ than WT CpG-injected mice, the recruitment of inflammatory myeloid cells and the decrease in resident macrophages were similar in these mice (Figure 4F). Accordingly, the concentrations of inflammatory chemokines in the sera of *Cxcr4*$^{+/1013}$ and WT CpG-injected mice increased similarly (Figure 4G). Furthermore, splenic pDCs from these mice overexpressed MHC2 and CD86 at equivalent levels (Figure 4H-I). Moreover, CD69^{+}-activated NK cells were also detected at similar frequencies in these mice (Figure 4J). Thus, despite a quantitative defect, pDC$^{+/1013}$ were recruited to the peritoneum, activated, and initiated systemic inflammation upon TLR9 engagement in vivo, as did pDC^{WT}, supporting that CXCR4 desensitization is dispensable for their innate functions.

CXCR4 dysfunction promotes skin inflammation without affecting DC activation

Given the skin-associated symptoms reported in WHIM patients, we next investigated the impact of CXCR4 dysfunction on skin DC subsets and LCs. We used HPV mice[47-49] to model HPV-induced dysplasia and chronic inflammation. The increase in flank epidermal thickness observed in HPV mice was worsened in HPV+/1013 mice (Figure 5A) and associated with higher numbers of dermal CD3^{dim} T cells than in HPV mice (supplemental Figure 5A-C),[47,52] suggesting greater inflammation in the skin of HPV+/1013 than HPV mice. LC density was diminished in the epidermal sheets in the context of HPV-induced dysplasia and their round morphology with short dendrites reflected their activation, independently of CXCR4 functioning (Figure 5B). We next analyzed DC subsets and LCs in skin cell suspensions (supplemental Figure 5D). pDCs were very rare in these suspensions, regardless of mouse genotype (not shown). HPV-induced dysplasia led to an accumulation of cDC subsets and LCs (Figure 5D). The frequency and number of cDC1, cDC2, and LCs among CD45^{+} cells did not differ according to CXCR4 genotype, although cDC1 and LCs tended to accumulate more in HPV+/1013 than HPV mice (Figure 5C-D). In the context of HPV, MHC2 expression was reduced in cDCs and LCs (Figure 5E-F, upper). CD80 expression was upregulated in cDC1, cDC2, and LCs from HPV and HPV+/1013 mice, as was that of CD86 in LCs and cDC1 (Figure 5E-F, middle and lower). Overall, these results show that the skin-DC compartment is generally preserved in the *Cxcr4*$^{+/1013}$ context, despite the worsening of HPV-associated skin inflammation.

Skin DC and LC migration is impaired by CXCR4 dysfunction

We next assessed the impact of CXCR4 dysfunction on the migration of skin DCs to SDLNs (Figure 6A). Both the frequency and number of migDCs were lower in the SDLNs of *Cxcr4*$^{+/1013}$ and HPV+/1013 mice than those of their control counterparts (Figure 6A-C). We performed FITC painting experiments to determine whether the reduction in migDC$^{+/1013}$ numbers resulted from a migration defect (Figure 6D). The number of FITC^{+} migDC1 and migDC2+LC recovered from the SDLNs of *Cxcr4*$^{+/1013}$ mice was reduced (Figure 6E), similarly to that of the FITC^{-} DCs. This diminution was not associated with reduced CCR7 or CXCR4 expression (Figure 6F). We next tested whether CXCR4 blockade would restore *Cxcr4*$^{+/1013}$ DC migration. AMD3100 injection reduced the migration of migDC^{WT} to SDLNs, whereas no increase

Figure 3 (continued) spleen, and BM from each parabiont. pDC was defined as live CD3^{-}Ly6G^{-}CD11b^{-}CD115^{-}CD11c^{lo}CD317^{+}Ly6C^{+}B220^{+} cells and Ly6C^{lo} monocytes as live CD3^{-}B220^{-}Ly6G^{-}CD115^{+}CD11b^{+}CD317^{-}Ly6C^{lo} cells. (F) Spleen/blood ratios of WT and *Cxcr4*$^{+/1013}$ pDCs and Ly6C^{lo} monocytes calculated for the spleen of WT (white background) and *Cxcr4*$^{+/1013}$ (gray background) parabionts (mean ± SEM, n = 5 pairs of mice). Mice had a C57BL/6J genetic background. Statistical analysis was performed using the paired *t* test. $^{*}P < .05$, $^{**}P < .01$, $^{****}P < .001$.

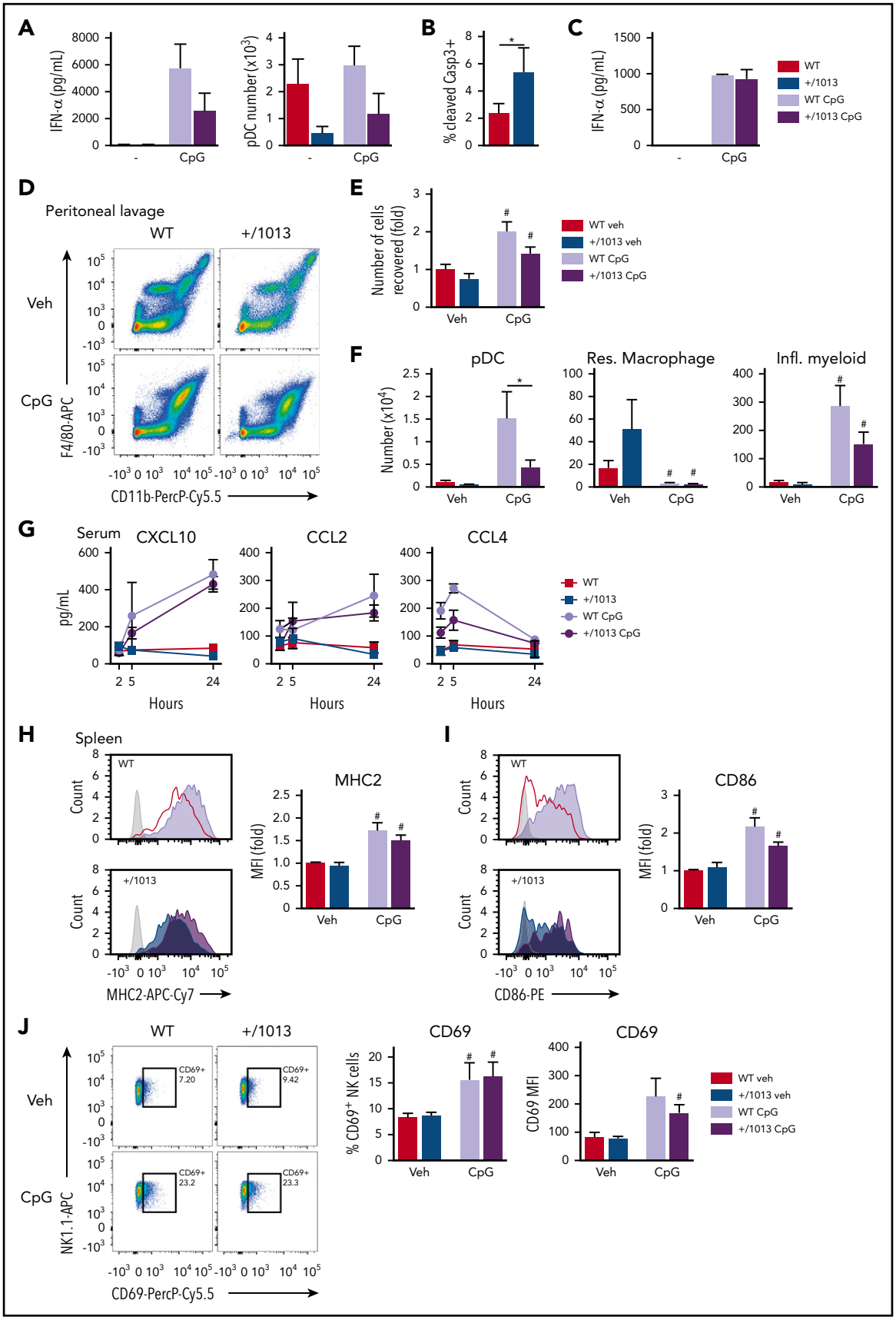

Figure 4. CXCR4 dysfunction does not alter pDC function. (A) IFN-α secretion (left) by splenic pDC from +/1013 and WT mice stimulated with CpG-ODN (CpG) or not (−) for 18 hours. pDC numbers (right) at the end of the culture. Mean ± SEM, n = 5-6 per group, cumulative data from 2 experiments. (B) Cleaved Caspase 3 levels in freshly isolated spleen pDCs (live CD11c^{int}CD317^{+} cells) from +/1013 and WT mice. Mean ± SEM, n = 9 per group, cumulative data from 3 experiments. (C) IFN-α secretion by Flt3-L-derived

in migDC$^{+/1013}$ migration could be observed (Figure 6G). Overall, these results show that dysfunctional CXCR4 signal termination impairs skin-DC migration to and/or their entry into SDLNs at steady state, as well as in acute and chronic inflammation.

CXCR4 dysfunction fosters the arrival of highly activated migDCs to SDLNs

We further investigated the role of CXCR4 in the activation of migDCs. MigDCs from HPV mice (migDC^{HPV}) showed lower MHC2 levels than migDC^{WT} (Figure 7A-B), consistent with previous reports.[59,60] ResDC^{HPV} and pDC^{HPV} also showed lower MHC2 levels than their controls (Figure 7B-C), highlighting a systemic effect of HPV-induced inflammation on DC-subset activation. In contrast, MHC2 levels were not decreased in migDCs from HPV+/1013 mice (migDC$^{HPV+/1013}$), resDC$^{HPV+/1013}$, and pDC$^{HPV+/1013}$. Moreover, migDC$^{HPV+/1013}$ showed an activated phenotype, with higher levels of CD80 and CD86 than migDC^{HPV}. Such an increase in costimulatory molecule expression, as well as that of CCR7, affected both migDC1 and migDC2+LC, although it was statistically significant only for migDC1 (Figure 7D). Remarkably, this pattern was also found in migDC$^{+/1013}$, suggesting that it did not result from the increased skin inflammation observed in HPV+/1013 mice (supplemental Figure 5). This prompted us to investigate whether DC$^{+/1013}$ were intrinsically more prone to activation than DC^{WT}. cDC1-like and cDC2-like BMDC$^{+/1013}$ and BMDC^{WT} were similarly activated by TLR4 and TLR8 agonists, whether or not CXCL12 was added to the culture medium (Figure 7E). Overall, these experiments suggest that the increased activation of migDC$^{+/1013}$ does not result from an intrinsically higher capacity to become activated, but rather from their altered migration dynamics.

Discussion

We used patient-derived CXCR4 dysfunction, associated with a high susceptibility to HPV pathogenesis, to investigate the role of CXCR4 in DC biology. Our results identify prominent and subset-specific effects of CXCR4 signal termination on DC distribution and function that underpin adequate immune homeostasis and function. They suggest that the CXCL12/CXCR4 signaling axis sets a threshold for both pDC egress from the BM and LC/cDC migration from the dermis to SDLNs, which has a profound impact on migDC activation.

We provide the demonstration that CXCR4 activity regulates the abundance of peripheral pDCs, both in humans and mice, presumably through the control of pDC egress from the BM, while not altering their entry into the spleen nor residency. We rule out the hypothesis that reduced peripheral pDC$^{+/1013}$ results from a defect in their production because their frequency was higher and their number preserved in the BM. Nevertheless, a bias toward myeloid-derived pDC differentiation[7] could explain the lower SiglecH levels in splenic pDC$^{+/1013}$ than pDC^{WT}. Chopin et al[31] reported that the level of CXCR4 expression by pDCs regulates their retention in the BM. Our study shows that the WS-associated CXCR4 dysfunction mimics the consequences of defective CXCR4 downregulation,[31] thus highlighting the critical importance of the proper regulation of the CXCR4 signaling in pDC trafficking. In a model of CpG-induced inflammation that strictly depends on pDC,[56] we demonstrate that pDC$^{+/1013}$ can be mobilized and activated in vivo, induce inflammatory responses, and activate NK cells to the same extent as pDC^{WT}. In addition, pDC$^{+/1013}$ produced IFN-α as efficiently as pDC^{WT} upon TLR9 engagement. Thus, our results do not support intrinsic pDC dysfunction as the mechanism contributing to WHIM patients' susceptibility to infectious diseases, although reduced pDC numbers early in the course of infection may delay the mounting of an immune response.

Although our report is in accordance with previous findings of Tassone et al concerning the reduction of peripheral pDCs, it contradicts their conclusion that circulating cDC frequency and number are reduced in WHIM patients.[44] Indeed, we show the frequency to be elevated for cDC1 and normal for cDC2 in WHIM patients relative to healthy donors. cDC numbers were preserved as well. Different factors might explain this discrepancy. First, we used an antibody panel including anti-CD11c, anti-HLA-DR, anti-CD1c, and anti-CD141 antibodies to gate on cDC subsets, whereas Tassone et al used anti-CD4 and anti-CD1c antibodies to identify cDCs. Second, we have worked on whole blood and not on isolated peripheral blood mononuclear cells. Moreover, we cannot rule out that differences in patient treatment might affect cDC concentrations. Supporting our data in humans, the cDC frequency was elevated in the spleens of *Cxcr4*$^{+/1013}$ mice. These results are consistent with preserved myeloid differentiation and may also partially result from the local extramedullary hematopoiesis reported for these mice.[46] Our data further show that the number, but not frequency, of circulating pre-cDCs was reduced by CXCR4 dysfunction, consistent with the role reported for CXCR4 in their medullar retention.[32,61] Nevertheless, the resDC compartment was globally preserved in both lymphoid and nonlymphoid tissues from *Cxcr4*$^{+/1013}$ mice, in support of efficient local differentiation of pre-cDCs and, in the skin, as a possible result of cDC entrapment and accumulation.

WHIM patients suffer from severe HPV-induced warts.[38,41-43] We show that WS-associated CXCR4 dysfunction is associated with a marked reduction in DC and LC migration from the skin to SDLNs. Remarkably, CXCR4 blockade in control mice similarly induced a reduction in skin DC migration. Thus, although CXCR4 promotes skin DC migration to SDLNs as previously reported by Kabashima et al,[26] the WS-associated gain of CXCR4 function completely abrogates this pro-migratory effect. Our interpretation of this

Figure 4 (continued) pDCs from +/1013 and WT mice stimulated with CpG-ODN for 18 hours. Mean ± SEM, n = 2 per group, cumulative data from 2 experiments. (D-J) +/1013 and WT mice were injected with CpG-DOTAP (CpG) or DOTAP only (vehicle [veh]). (D) Representative dot plot of the CD45$^+$ cells recovered in the peritoneal lavage 24 hours after treatment. (E) Fold increase in the number of cells recovered in the peritoneal lavage, the reference being the WT veh mice. (F) Number of pDCs (live CD45$^+$CD11b$^-$F4/80$^-$CD11c^{lo}Ly6C$^+$CD317$^+$B220$^+$ cells), resident macrophages (live CD45$^+$CD11b^{hi}F4/80^{hi}Ly6G$^-$Ly6C$^{int\ to\ hi}$ cells), and inflammatory myeloid cells (live Infl. myeloid, CD45$^+$B220$^-$CD11b$^+$F4/80$^{lo\ to\ +}$Ly6C^{hi} cells) in the peritoneal lavage. (G) Serum cytokine levels at different timepoints. (H-I) Surface expression of MHC2 (H) and CD86 (I) by splenic pDC (CD11c^{int}CD317$^+$B220$^+$). Representative histograms (left) and the fold increase in the MFI relative to WT veh mice (right) are shown. The gray histogram corresponds to isotype control. (J) Surface expression of CD69 by splenic NK cells (live CD3$^-$NK1.1$^+$CD49b$^+$ cells). Representative dot plots (left), the percentage of CD69$^+$ NK cells (middle), and CD69 MFI (right) are shown.) Mean ± SEM, n = 5-6 per group, cumulative data from 3 experiments (D-J). Mice had a C57BL/6J genetic background. Statistical analysis was performed using the 2-tailed unpaired Mann-Whitney test to compare veh- and CpG-treated mice ($^{\#}P < .05$) or the WT and +/1013 groups ($^{*}P < .05$).

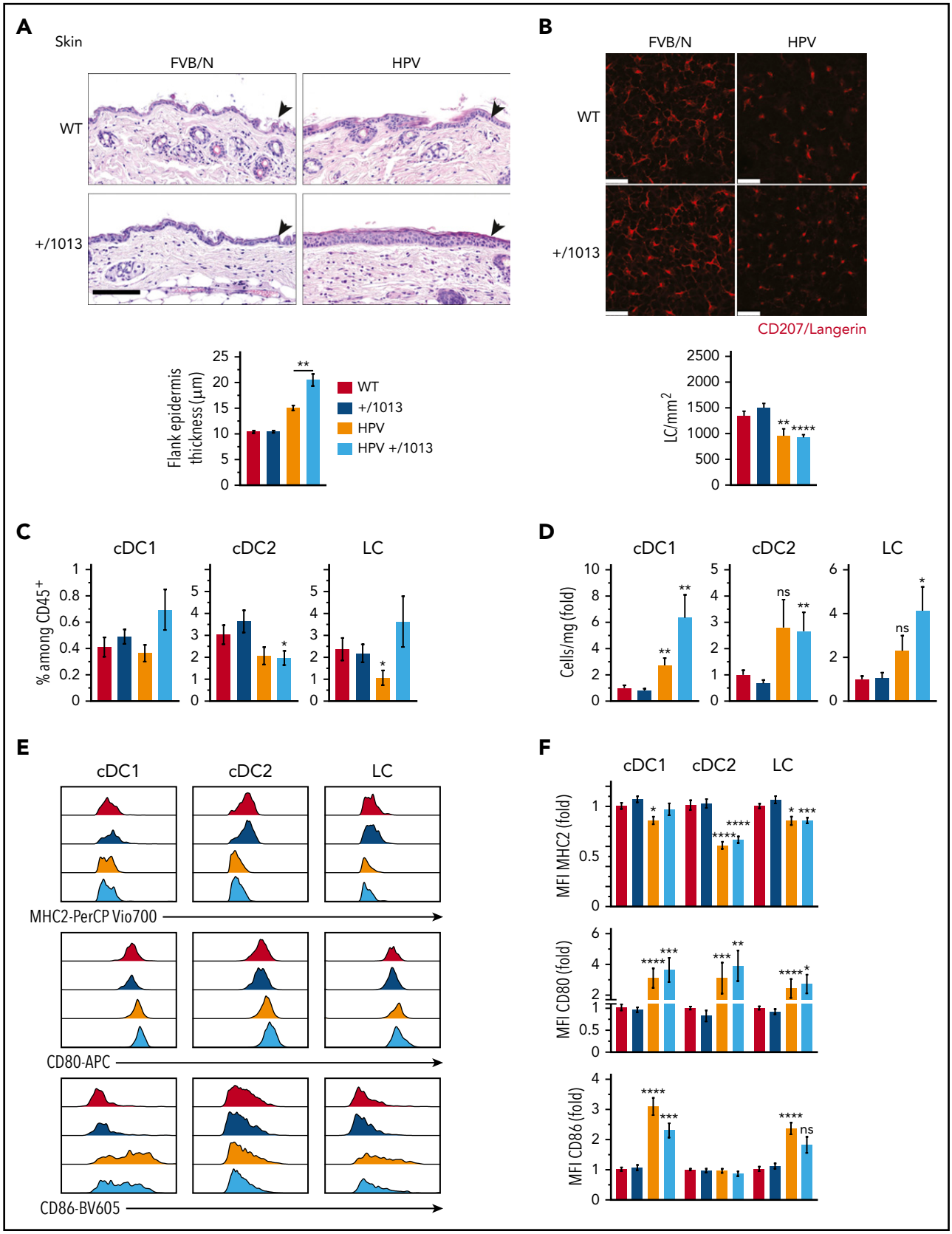

Figure 5. CXCR4 dysfunction promotes HPV-associated chronic inflammation while preserving DC subset activation. (A) Representative images for hematoxylin and eosin coloration of flank skin sections (upper). Epidermal (arrowheads) thickness was measured along the tissue, with at least 10 measurements per sample (lower, mean ± SEM, n = 6-8 mice). Scale bar, 100 µm. (B) Representative confocal microscopy images (top) from epidermal sheets stained for CD207 (red). $CD207^+$ cells were counted in 5 fields per sample (n = 3 samples per genotype) and the cell density calculated (bottom). Scale bars, 25 µm. (C) Percentage of cDC1, cDC2, and LCs among $CD45^+$ skin cells. (D) Number of cDC1,

apparently counterintuitive migration defect in *Cxcr4*$^{+/1013}$ mice is that DCs and LCs might be trapped in the dermis, where CXCL12 is produced,[23-28] despite their expression of CCR7, and as a consequence of a possibly skewed balance between several chemotactic signals. Indeed, Ricart et al reported that in vitro countergradients of CXCL12 and CCL19/CCL21 can result in the homing of DCs to a central zone, where chemokine-derived signals are balanced.[62] Moreover, the levels of CXCL12 were shown to be higher in the dermis of *Cxcr4*$^{+/1013}$ mice than that of their controls,[27] suggesting that DC$^{+/1013}$ entrapment could arise from the combined effect of high CXCL12 quantities in the dermis and exacerbated CXCR4-dependent signaling. Because CXCL12 is expressed by endothelial cells from the lymphatics,[26] migDC$^{+/1013}$ may also be trapped in these vessels on their way to LNs. Our results show that CCR7 expression is upregulated in migDC$^{+/1013}$ compared with migDC^{WT} in the HPV context, supporting the hypothesis that only the DCs that were highly responsive to CCL19/CCL21 signals could escape CXCL12 attraction in *Cxcr4*$^{+/1013}$ mice. That no CCR7 upregulation was detected in migDC$^{+/1013}$ in FITC-painting experiments suggests the contribution of other drivers of DC migration during acute inflammation. Importantly, CXCR4 blockade did not rescue migDC$^{+/1013}$ migration to SDLNs. This might reflect sequential roles for CXCR4 and CCR7 in guiding skin DC migration, or, alternatively, an abrogation of the cooperativity between CXCR4 and CCR7 that was previously reported in pDCs and T cells.[33,63] Overall, our data suggest that proper CXCR4 regulation controls skin immune homeostasis by setting up a threshold for cDC and LC migration from the dermis to SDLNs.

CXCR4 dysfunction is associated with profound alteration of the activation of the DC subsets and LCs recovered from SDLNs, with specific features in steady-state and chronic HPV-induced inflammation. First, CXCR4 dysfunction results in increased expression of costimulatory molecules by SDLN migDC, but not resDC or pDC. This occurs both at steady-state and in the context of HPV-induced inflammation, ruling out the possibility that the high activation level of migDC is simply because of the increased inflammation observed in the skin of HPV+/1013 mice. Upon in vitro stimulation, BMDC$^{+/1013}$ were similarly activated as BMDC^{WT}, suggesting that the increased activation of migDC$^{+/1013}$ in SDLNs is not intrinsically programmed. Accordingly, the skin DC and LC phenotype was similar in HPV and HPV+/1013 mice. Thus, we propose that the high expression of costimulatory molecules by migDC$^{+/1013}$ results from the stringent selection of DCs exiting the skin, meaning that only the most activated cells would leave the CXCL12-enriched dermis and reach the LNs. Second, CXCR4 dysfunction also markedly affects MHC2 expression by SDLN DCs in the context of chronic inflammation. Indeed, HPV-induced inflammation was associated with marked downregulation of MHC2 expression by skin DCs, as expected from previous studies,[59,60] and independently of CXCR4 status. Such a tolerogenic state of DCs was reported to promote skin graft tolerance[64] and could be a component of HPV immune-escape mechanisms. However, although MHC2 downregulation was also present in SDLN migDC^{HPV}, resDC^{HPV}, and pDC^{HPV}, this pattern was not found in any of these subsets in HPV+/1013 mice. This absence of a tolerogenic profile affecting all LN DC subsets may be a distal consequence of exacerbated skin inflammation in HPV+/1013 mice. Such worsening of HPV-induced pathogenesis may arise from the cumulative effects of the mutant CXCR4 procarcinogenetic properties in keratinocytes[65,66] and effect on stromal and immune cells, which could be further fostered by highly activated migDCs, promoting inflammation in HPV+/1013 mice.

Whether alterations in DC biology directly contribute to the high susceptibility of WHIM patients to HPV-induced pathogenesis remains to be investigated. One may hypothesize that inefficient priming of HPV-specific T-cell responses resulting from scarce numbers of DCs reaching the LN,[67] combined with defective DC–T-cell interactions when T cells express WS-associated CXCR4 mutations,[68] could hamper lesion control.[69] Moreover, excessively activated DCs could be defective for CD8 T-cell preconditioning to become resident memory T cells[70] involved in the local control of HPV,[71] prime inappropriate T-cell responses, or fail in inducing tolerance.[72,73] In support of the hypothesis that CXCR4 dysfunction can exacerbate immune responses, an increase in the generation of plasma cells was reported in the SLO of *Cxcr4*$^{+/1013}$ mice, although it did not result in long-term protective humoral immunity.[74] This raises the possibility that WHIM patients might paradoxically suffer from a lack of tolerance toward their skin microbiota, which includes the HPV virome,[75,76] combined with defects in the mounting of anti-infectious immune responses. Further studies are needed to test these hypotheses, which may be conducted using mouse models of papillomavirus infection.[77,78]

Our work suggests that functional restoration of the DC compartment might have contributed to the spontaneous cure of HPV-induced warts reported in a WHIM patient who fortuitously lost the mutated *CXCR4* allele in a single myeloid progenitor that eventually repopulated the myeloid repertoire.[39] Indeed, the critical role of DCs in the priming of adaptive immune responses argues in favor of a contribution of the recovery of skin DC migration to the beneficial effects of this chromothriptic event.[79] Our work also suggests that normalizing DC subsets trafficking, together with their activation, could be among the mechanisms accounting for the beneficial effects of the treatment of WHIM patients with AMD3100 combined with imiquimod on HPV-induced lesions and HPV cancer progression.[42,80]

In summary, our work provides mechanistic cues to explain the physiopathology of WS and unravels the profound impact of CXCR4-dependent signal termination on DC subsets migration dynamics and activation state.

Figure 5 (continued) cDC2, and LC per milligram of skin as the fold change relative to WT (see supplemental Figure 5 for the gating strategy, mean ± SEM, n = 9-11 per group, cumulative data from 4 independent experiments). (E) Representative histograms showing the surface expression of MHC2, CD80, and CD86 by cDC1, cDC2, and LCs from WT, +/1013, HPV, and HPV+/1013 mice. (F) Bar graphs show the expression of MHC2, CD80, and CD86 as the fold change relative to WT (mean ± SEM, n = 10-12 mice/group for MHC2 from 5 experiments, n = 9-11 mice/group for CD86 from 4 experiments, n = 7-9 mice/group for CD80 from 3 experiments). Mice had an FVB/N genetic background. Statistical analysis was performed using the 2-tailed, unpaired Mann-Whitney test to compare HPV mice and HPV+/1013 genotypes (A, $^{**}P < .01$) or HPV and HPV+/1013 mice to their non-HPV counterparts (B-E, $^{*}P < .05$, $^{**}P < .01$, $^{***}P < .005$, $^{****}P < .001$).

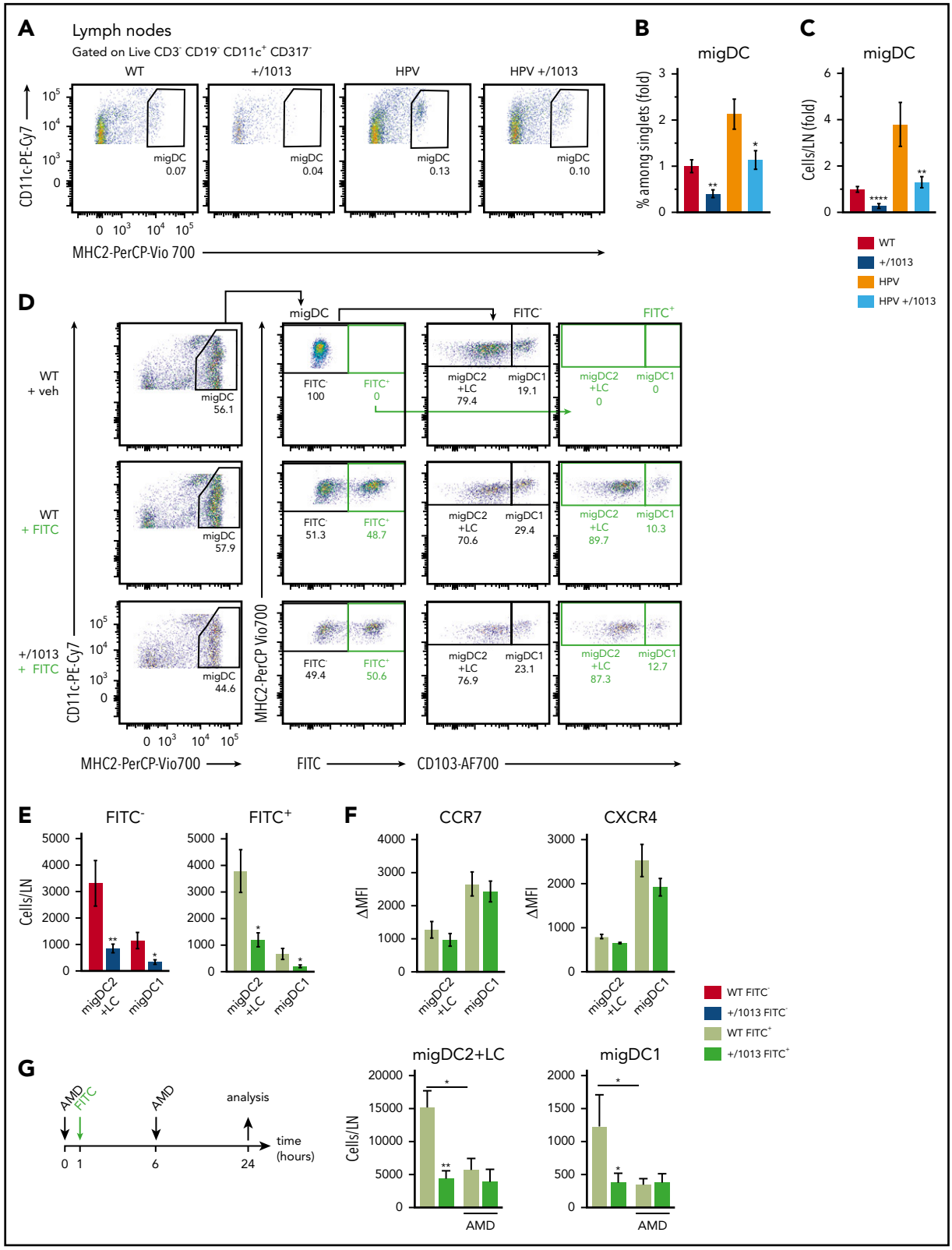

Figure 6. CXCR4 controls steady-state skin DC migration and in acute inflammation. (A) Representative dot plots showing migDCs ($CD11c^+MHC2^{hi}$ gated on $CD3^-CD19^-CD317^-$) in inguinal LNs from WT, +/1013, HPV, and HPV+/1013 mice. Percentages among parent cells are indicated. (B-C) Percentage among singlets (B) and number (C) of migDCs per LN as the fold change relative to WT values. (B-C) Mean ± SEM, n = 10-11 per group, cumulative data from four independent experiments. (D) Representative dot plots showing the gating strategy for identifying $CD103^+$ migDC1 and $CD103^-$ migDC2+LC subsets in SDLNs from mice 24 hours after FITC treatment. (E) Number of FITC-negative ($FITC^-$) and FITC-positive ($FITC^+$) migDCs in skin-draining LNs from FITC-treated mice. (F) Membrane expression of CCR7 (left) and CXCR4 (right) by $FITC^+$ migDC1 and migDC2+LC from WT and +/1013 mice. (G) Left, experimental design: mice received AMD3100 or PBS at t = 0 and 6 hours. FITC was applied at t = 1 hour. Right, number of $FITC^+$ migDC1 and migDC2+LC in inguinal LNs form mice treated or not with AMD3100 (AMD). Mean ± SEM, n = 8-9 mice/group, cumulative data from 2 independent experiments (D-F). Mean ± SEM, n = 6-8 mice/group, cumulative data from 3 independent experiments (G). Mice had an FVB/N genetic background. Statistical analysis was performed using the 2-tailed, unpaired Mann-Whitney test to compare WT and +/1013 mice. $*P < .05$, $**P < .01$.

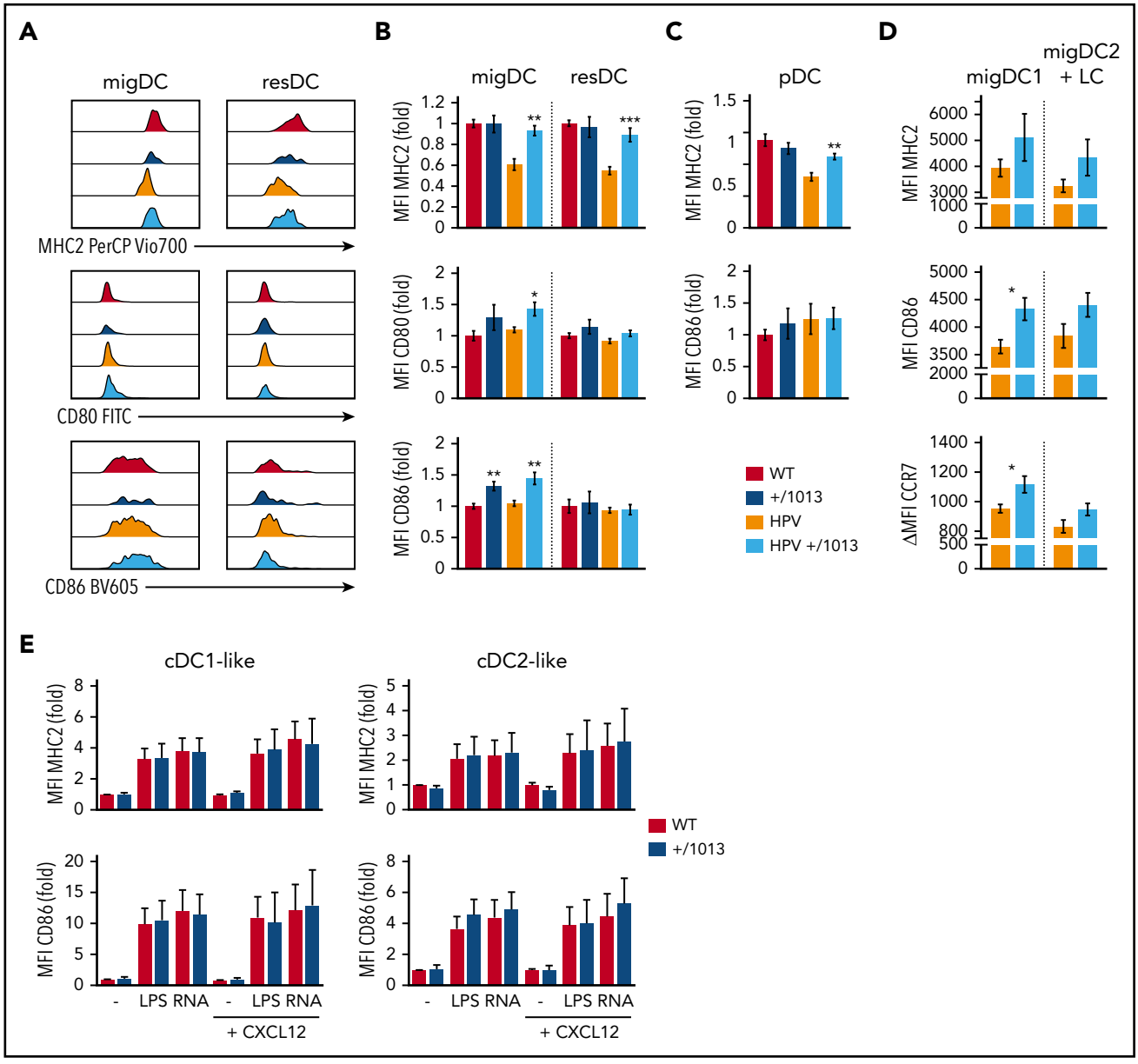

Figure 7. CXCR4 dysfunction promotes steady-state DC activation and in the context of HPV-associated inflammation. (A) Representative histograms showing the levels of MHC2, CD80, and CD86 surface expression by migDCs and resDCs (defined as $CD11c^{+}MHC2^{hi}$ and $CD11c^{hi}MHC2^{+}$ gated on live $CD3^{-}CD19^{-}CD317^{-}$ cells, respectively) recovered from the SDLNs of WT, +/1013, HPV, and HPV+/1013 mice. (B) Bar graphs showing the surface expression of MHC2, CD80, and CD86 for migDCs and resDCs as the fold change relative to WT. (C) Bar graphs showing the expression of MHC2 and CD86 in pDCs as the fold change relative to WT. Mean ± SEM, n = 8-11 mice/group from 4 experiments for MHC2, n = 8 mice/group from 3 experiments for CD86, n = 6 mice/group from 2 experiments for CD80 (B-C). (D) Bar graphs showing the surface expression of MHC2, CD86, and CCR7 for migDC1 and migDC2+LC from HPV and HPV+/1013 mice (mean ± SEM, n = 6-7 per group from 1 of 2 representative experiments). (E) Bar graphs showing the surface expression of MHC2 and CD86 upon LPS or ssRNA stimulation for DC1-like and DC2-like BMDCs derived from WT and +/1013 mice. Results are expressed as the fold change relative to nontreated WT (mean ± SEM, cumulative data from n = 4 to 5 independent experiments). Mice had an FVB/N genetic background. Statistical analysis was performed using the 2-tailed, unpaired Mann-Whitney test to compare +/1013 mice to their WT counterparts. $^{**}P < .01$, $^{***}P < .005$.

Acknowledgments

The authors thank Hélène Gary (Plaimmo, Unité Mixte de Service/Institut Paris-Sud d'Innovation Thérapeutique [UMS/IPSIT], Châtenay-Malabry, France), Sarah Mendez, Baptiste Lecomte (Animex, UMS/IPSIT), and Khadidiatou Kouyate (Laboratory "Inflammation, Microbiome and Immunosurveillance") for excellent technical assistance. The authors also thank Floriane Meuris for backcrossing the *Cxcr4*$^{+/1013}$ mice onto the FVB/N genetic background and are grateful to Matthieu Bertrand, Patrice Hémon, and Chloé Lourenço for performing preliminary experiments.

This work was supported by grants from the ERA-Net Infect-ERA "HPV-MOTIVA" (Agence Nationale de la Recherche [ANR]-15-IFEC-0004-01) (F.B. and G.S.L.), MSCA-ITN-2014-ETN/Marie Skłodowska-Curie Innovative Training Networks (ITN-ETN) "ONCOgenic Receptor Network of Excellence and Training" (H2020-MSCA Program, grant agreement 641833-ONCORNET) (F.B. and G.S.L.), the "Fondation ARC pour la Recherche sur le Cancer" (G.S.L.), LabEx LERMIT (Laboratory of Excellence in Research on Medication and Innovative Therapeutics) (ANR-10-LABX-33) under the program "Investissements d'Avenir" (ANR-11-IDEX-0003-01) (F.B. and G.S.L.), and ANR Projet de Recherche Collaborative (PRC) grant ANR-17-CE14-0019 (K.B.). C.G. was supported by the MSCA-ITN-2014-ETN/ITN-ETN "ONCOgenic Receptor Network of Excellence and Training" and the Fondation pour la Recherche Médicale (FDT201805005700). M.V. and J.C. were supported by a doctoral fellowship from the Doctoral School "Innovation Thérapeutique du Fondamental à l'Appliqué" (ED 569). M.V.

was supported by the "Ligue contre le Cancer" (IP/SC-15956). N.P. was supported by a postdoctoral fellowship from the Région Ile de France (Domaine d'Intérêt Majeur [DIM] Maladies Infectieuses, Parasitaires et Nosocomiales Emergentes).

Authorship

Contribution: C.G. and M.V. designed and performed experiments, analyzed data, contributed to writing the manuscript, and worked as co-first authors, a position assigned on the basis of the number of experiements performed, analysed, and interpreted, as well as the contribution to the setting up of the techniques used; J.C., M.R., M.-L.A., N.P., M.E., and M.L. designed and performed experiments and analyzed data; V.M.-E. designed and performed experiments with patient samples, analyzed data, and contributed to writing the manuscript; F.M.-N. performed histology experiments and analyzed data; Y.B., F.S., and J.D. provided blood samples from healthy donors and WHIM patients and reviewed the manuscript; L.G.N. provided access to the parabiosis data and reviewed the manuscript; K.B. reviewed the manuscript; F.B. helped with the study design, data analysis, and writing of the manuscript and procured funding for the study; and G.S.-L. conceived and supervised the study, designed and performed experiments, analyzed data, procured funding for the study, and wrote the manuscript.

Conflict-of-interest disclosure: The authors declare no competing financial interests.

ORCID profiles: C.G., 0000-0003-0180-5671; M.V., 0000-0001-5503-4900; M.E., 0000-0002-2105-1160; N.P., 0000-0002-2379-4945; F.S., 0000-0002-3537-9052; J.D., 0000-0002-4485-146X; K.B., 0000-0002-0534-3198; G.S.-L., 0000-0002-7924-5371.

Correspondence: Géraldine Schlecht-Louf, INSERM UMR 996, 32 rue des Carnets, 92140 Clamart, France; e-mail: geraldine.schlecht-louf@universite-paris-saclay.fr.

Footnotes

Submitted 29 April 2020; accepted 20 December 2020; prepublished online on *Blood* First Edition 22 January 2021. DOI 10.1182/blood.2020006675.

*C.G. and M.V. are co-first authors.

†J.C. and M.R. are co-second authors.

For original data, please contact Géraldine Schlecht Louf (geraldine.schlecht-louf@universite-paris-saclay.fr).

The online version of this article contains a data supplement.

There is a *Blood* Commentary on this article in this issue.

The publication costs of this article were defrayed in part by page charge payment. Therefore, and solely to indicate this fact, this article is hereby marked "advertisement" in accordance with 18 USC section 1734.

REFERENCES

1. Steinman RM, Banchereau J. Taking dendritic cells into medicine. *Nature*. 2007;449(7161):419-426.
2. Guilliams M, Dutertre CA, Scott CL, et al. Unsupervised high-dimensional analysis aligns dendritic cells across tissues and species. *Immunity*. 2016;45(3):669-684.
3. Merad M, Sathe P, Helft J, Miller J, Mortha A. The dendritic cell lineage: ontogeny and function of dendritic cells and their subsets in the steady state and the inflamed setting. *Annu Rev Immunol*. 2013;31(1):563-604.
4. Brown CC, Gudjonson H, Pritykin Y, et al. Transcriptional basis of mouse and human dendritic cell heterogeneity. *Cell*. 2019;179(4):846-863.e24.
5. Reizis B. Plasmacytoid dendritic cells: development, regulation, and function. *Immunity*. 2019;50(1):37-50.
6. Dress RJ, Dutertre CA, Giladi A, et al. Plasmacytoid dendritic cells develop from Ly6D^{+} lymphoid progenitors distinct from the myeloid lineage. *Nat Immunol*. 2019;20(7):852-864.
7. Rodrigues PF, Alberti-Servera L, Eremin A, Grajales-Reyes GE, Ivanek R, Tussiwand R. Distinct progenitor lineages contribute to the heterogeneity of plasmacytoid dendritic cells. *Nat Immunol*. 2018;19(7):711-722.
8. Murphy TL, Grajales-Reyes GE, Wu X, et al. Transcriptional control of dendritic cell development. *Annu Rev Immunol*. 2016;34(1):93-119.
9. Hoeffel G, Wang Y, Greter M, et al. Adult Langerhans cells derive predominantly from embryonic fetal liver monocytes with a minor contribution of yolk sac-derived macrophages. *J Exp Med*. 2012;209(6):1167-1181.
10. Swiecki M, Colonna M. The multifaceted biology of plasmacytoid dendritic cells. *Nat Rev Immunol*. 2015;15(8):471-485.
11. Alvarez D, Vollmann EH, von Andrian UH. Mechanisms and consequences of dendritic cell migration. *Immunity*. 2008;29(3):325-342.
12. Worbs T, Hammerschmidt SI, Förster R. Dendritic cell migration in health and disease. *Nat Rev Immunol*. 2017;17(1):30-48.
13. Eisenbarth SC. Dendritic cell subsets in T cell programming: location dictates function. *Nat Rev Immunol*. 2019;19(2):89-103.
14. Tiberio L, Del Prete A, Schioppa T, Sozio F, Bosisio D, Sozzani S. Chemokine and chemotactic signals in dendritic cell migration. *Cell Mol Immunol*. 2018;15(4):346-352.
15. Ohl L, Mohaupt M, Czeloth N, et al. CCR7 governs skin dendritic cell migration under inflammatory and steady-state conditions. *Immunity*. 2004;21(2):279-288.
16. Martln-Fontecha A, Sebastiani S, Höpken UE, et al. Regulation of dendritic cell migration to the draining lymph node: impact on T lymphocyte traffic and priming. *J Exp Med*. 2003;198(4):615-621.
17. Gunn MD, Kyuwa S, Tam C, et al. Mice lacking expression of secondary lymphoid organ chemokine have defects in lymphocyte homing and dendritic cell localization. *J Exp Med*. 1999;189(3):451-460.
18. Luther SA, Bidgol A, Hargreaves DC, et al. Differing activities of homeostatic chemokines CCL19, CCL21, and CXCL12 in lymphocyte and dendritic cell recruitment and lymphoid neogenesis. *J Immunol*. 2002;169(1):424-433.
19. Stutte S, Quast T, Gerbitzki N, et al. Requirement of CCL17 for CCR7- and CXCR4-dependent migration of cutaneous dendritic cells. *Proc Natl Acad Sci USA*. 2010;107(19):8736-8741.
20. Vanbervliet B, Bendriss-Vermare N, Massacrier C, et al. The inducible CXCR3 ligands control plasmacytoid dendritic cell responsiveness to the constitutive chemokine stromal cell-derived factor 1 (SDF-1)/CXCL12. *J Exp Med*. 2003;198(5):823-830.
21. Nagasawa T, Hirota S, Tachibana K, et al. Defects of B-cell lymphopoiesis and bone-marrow myelopoiesis in mice lacking the CXC chemokine PBSF/SDF-1. *Nature*. 1996;382(6592):635-638.
22. Uhlén M, Fagerberg L, Hallström BM, et al. Proteomics. Tissue-based map of the human proteome. *Science*. 2015;347(6220):1260419.
23. Pablos JL, Amara A, Bouloc A, et al. Stromal-cell derived factor is expressed by dendritic cells and endothelium in human skin. *Am J Pathol*. 1999;155(5):1577-1586.
24. Avniel S, Arik Z, Maly A, et al. Involvement of the CXCL12/CXCR4 pathway in the recovery of skin following burns. *J Invest Dermatol*. 2006;126(2):468-476.
25. Balabanian K, Lagane B, Pablos JL, et al. WHIM syndromes with different genetic anomalies are accounted for by impaired CXCR4 desensitization to CXCL12. *Blood*. 2005;105(6):2449-2457.
26. Kabashima K, Shiraishi N, Sugita K, et al. CXCL12-CXCR4 engagement is required for migration of cutaneous dendritic cells. *Am J Pathol*. 2007;171(4):1249-1257.
27. Pionnier N, Brotin E, Karadjian G, et al. Neutropenic mice provide insight into the role of skin-infiltrating neutrophils in the host protective immunity against filarial infective larvae. *PLoS Negl Trop Dis*. 2016;10(4):e0004605.

28. Gombert M, Dieu-Nosjean MC, Winterberg F, et al. CCL1-CCR8 interactions: an axis mediating the recruitment of T cells and Langerhans-type dendritic cells to sites of atopic skin inflammation. *J Immunol*. 2005; 174(8):5082-5091.

29. Kohara H, Omatsu Y, Sugiyama T, Noda M, Fujii N, Nagasawa T. Development of plasmacytoid dendritic cells in bone marrow stromal cell niches requires CXCL12-CXCR4 chemokine signaling. *Blood*. 2007;110(13): 4153-4160.

30. Minami H, Nagaharu K, Nakamori Y, et al. CXCL12-CXCR4 axis is required for contact-mediated human B lymphoid and plasmacytoid dendritic cell differentiation but not T lymphoid generation. *J Immunol*. 2017;199(7): 2343-2355.

31. Chopin M, Preston SP, Lun ATL, et al. RUNX2 mediates plasmacytoid dendritic cell egress from the bone marrow and controls viral immunity. *Cell Rep*. 2016;15(4):866-878.

32. Nakano H, Lyons-Cohen MR, Whitehead GS, Nakano K, Cook DN. Distinct functions of CXCR4, CCR2, and CX3CR1 direct dendritic cell precursors from the bone marrow to the lung. *J Leukoc Biol*. 2017;101(5):1143-1153.

33. Umemoto E, Otani K, Ikeno T, et al. Constitutive plasmacytoid dendritic cell migration to the splenic white pulp is cooperatively regulated by CCR7- and CXCR4-mediated signaling. *J Immunol*. 2012;189(1):191-199.

34. Ouwehand K, Santegoets SJ, Bruynzeel DP, Scheper RJ, de Gruijl TD, Gibbs S. CXCL12 is essential for migration of activated Langerhans cells from epidermis to dermis. *Eur J Immunol*. 2008;38(11):3050-3059.

35. Hernandez PA, Gorlin RJ, Lukens JN, et al. Mutations in the chemokine receptor gene CXCR4 are associated with WHIM syndrome, a combined immunodeficiency disease. *Nat Genet*. 2003;34(1):70-74.

36. Lagane B, Chow KY, Balabanian K, et al. CXCR4 dimerization and beta-arrestin-mediated signaling account for the enhanced chemotaxis to CXCL12 in WHIM syndrome. *Blood*. 2008;112(1):34-44.

37. Bachelerie F. CXCL12/CXCR4-axis dysfunctions: markers of the rare immunodeficiency disorder WHIM syndrome. *Dis Markers*. 2010; 29(3-4):189-198.

38. Dotta L, Tassone L, Badolato R. Clinical and genetic features of warts, hypogammaglobulinemia, infections and myelokathexis (WHIM) syndrome. *Curr Mol Med*. 2011;11(4):317-325.

39. McDermott DH, Gao JL, Liu Q, et al. Chromothriptic cure of WHIM syndrome. *Cell*. 2015;160(4):686-699.

40. Levoye A, Balabanian K, Baleux F, Bachelerie F, Lagane B. CXCR7 heterodimerizes with CXCR4 and regulates CXCL12-mediated G protein signaling. *Blood*. 2009;113(24): 6085-6093.

41. Beaussant Cohen S, Fenneteau O, Plouvier E, et al. Description and outcome of a cohort of 8 patients with WHIM syndrome from the French Severe Chronic Neutropenia Registry. *Orphanet J Rare Dis*. 2012;7(1):71.

42. McDermott DH, Murphy PM. WHIM syndrome: immunopathogenesis, treatment and cure strategies. *Immunol Rev*. 2019;287(1): 91-102.

43. Dotta L, Notarangelo LD, Moratto D, et al. Long-term outcome of WHIM syndrome in 18 patients: high risk of lung disease and HPV-related malignancies. *J Allergy Clin Immunol Pract*. 2019;7(5):1568-1577.

44. Tassone L, Moratto D, Vermi W, et al. Defect of plasmacytoid dendritic cells in warts, hypogammaglobulinemia, infections, myelokathexis (WHIM) syndrome patients. *Blood*. 2010;116(23):4870-4873.

45. Balabanian K, Brotin E, Biajoux V, et al. Proper desensitization of CXCR4 is required for lymphocyte development and peripheral compartmentalization in mice. *Blood*. 2012; 119(24):5722-5730.

46. Freitas C, Wittner M, Nguyen J, et al. Lymphoid differentiation of hematopoietic stem cells requires efficient Cxcr4 desensitization. *J Exp Med*. 2017;214(7): 2023-2040.

47. Meuris F, Gaudin F, Aknin ML, Hémon P, Berrebi D, Bachelerie F. Symptomatic Improvement in human papillomavirus-induced epithelial neoplasia by specific targeting of the CXCR4 chemokine receptor. *J Invest Dermatol*. 2016;136(2):473-480.

48. Arbeit JM, Münger K, Howley PM, Hanahan D. Progressive squamous epithelial neoplasia in K14-human papillomavirus type 16 transgenic mice. *J Virol*. 1994;68(7):4358-4368.

49. Coussens LM, Hanahan D, Arbeit JM. Genetic predisposition and parameters of malignant progression in K14-HPV16 transgenic mice. *Am J Pathol*. 1996;149(6):1899-1917.

50. Chong SZ, Evrard M, Devi S, et al. CXCR4 identifies transitional bone marrow premonocytes that replenish the mature monocyte pool for peripheral responses. *J Exp Med*. 2016;213(11):2293-2314.

51. van Furth R, Sluiter W. Distribution of blood monocytes between a marginating and a circulating pool. *J Exp Med*. 1986;163(2): 474-479.

52. Van Hede D, Polese B, Humblet C, et al. Human papillomavirus oncoproteins induce a reorganization of epithelial-associated γδ T cells promoting tumor formation. *Proc Natl Acad Sci USA*. 2017;114(43):E9056-E9065.

53. Mouriès J, Moron G, Schlecht G, Escriou N, Dadaglio G, Leclerc C. Plasmacytoid dendritic cells efficiently cross-prime naive T cells in vivo after TLR activation. *Blood*. 2008;112(9): 3713-3722.

54. Brasel K, De Smedt T, Smith JL, Maliszewski CR. Generation of murine dendritic cells from flt3-ligand-supplemented bone marrow cultures. *Blood*. 2000;96(9):3029-3039.

55. Mayer CT, Ghorbani P, Nandan A, et al. Selective and efficient generation of functional Batf3-dependent CD103+ dendritic cells from mouse bone marrow. *Blood*. 2014; 124(20):3081-3091.

56. Guillerey C, Mouriès J, Polo G, et al. Pivotal role of plasmacytoid dendritic cells in inflammation and NK-cell responses after TLR9 triggering in mice. *Blood*. 2012;120(1):90-99.

57. Liu K, Victora GD, Schwickert TA, et al. In vivo analysis of dendritic cell development and homeostasis. *Science*. 2009;324(5925): 392-397.

58. Liu K, Waskow C, Liu X, Yao K, Hoh J, Nussenzweig M. Origin of dendritic cells in peripheral lymphoid organs of mice. *Nat Immunol*. 2007;8(6):578-583.

59. Mittal D, Kassianos AJ, Tran LS, et al. Indoleamine 2,3-dioxygenase activity contributes to local immune suppression in the skin expressing human papillomavirus oncoprotein e7. *J Invest Dermatol*. 2013;133(12): 2686-2694.

60. Chandra J, Miao Y, Romoff N, Frazer IH. Epithelium expressing the E7 oncoprotein of HPV16 attracts immune-modulatory dendritic cells to the skin and suppresses their antigen-processing capacity. *PLoS One*. 2016;11(3): e0152886.

61. Schmid MA, Takizawa H, Baumjohann DR, Saito Y, Manz MG. Bone marrow dendritic cell progenitors sense pathogens via Toll-like receptors and subsequently migrate to inflamed lymph nodes. *Blood*. 2011;118(18): 4829-4840.

62. Ricart BG, John B, Lee D, Hunter CA, Hammer DA. Dendritic cells distinguish individual chemokine signals through CCR7 and CXCR4. *J Immunol*. 2011;186(1):53-61.

63. Hayasaka H, Kobayashi D, Yoshimura H, Nakayama EE, Shioda T, Miyasaka M. The HIV-1 Gp120/CXCR4 axis promotes CCR7 ligand-dependent CD4 T cell migration: CCR7 homo- and CCR7/CXCR4 hetero-oligomer formation as a possible mechanism for up-regulation of functional CCR7. *PLoS One*. 2015;10(2):e0117454.

64. Matsumoto K, Leggatt GR, Zhong J, et al. Impaired antigen presentation and effectiveness of combined active/passive immunotherapy for epithelial tumors. *J Natl Cancer Inst*. 2004;96(21):1611-1619.

65. Meuris F, Carthagena L, Jaracz-Ros A, et al. The CXCL12/CXCR4 signaling pathway: a new susceptibility factor in human papillomavirus pathogenesis. *PLoS Pathog*. 2016;12(12): e1006039.

66. Chow KY, Brotin É, Ben Khalifa Y, et al. A pivotal role for CXCL12 signaling in HPV-mediated transformation of keratinocytes: clues to understanding HPV-pathogenesis in WHIM syndrome. *Cell Host Microbe*. 2010; 8(6):523-533.

67. Celli S, Day M, Müller AJ, Molina-Paris C, Lythe G, Bousso P. How many dendritic cells are required to initiate a T-cell response? *Blood*. 2012;120(19):3945-3948.

68. Kallikourdis M, Trovato AE, Anselmi F, et al. The CXCR4 mutations in WHIM syndrome impair the stability of the T-cell immunologic synapse. *Blood*. 2013;122(5):666-673.

69. Schiffman M, Doorbar J, Wentzensen N, et al. Carcinogenic human papillomavirus infection. *Nat Rev Dis Primers*. 2016;2(1):16086.

70. Mani V, Bromley SK, Äijö T, et al. Migratory DCs activate TGF-β to precondition naïve $CD8^+$ T cells for tissue-resident memory fate. *Science*. 2019;366(6462):eaav5728.

71. Strickley JD, Messerschmidt JL, Awad ME, et al. Immunity to commensal papillomaviruses protects against skin cancer. *Nature*. 2019;575(7783):519-522.

72. Audiger C, Rahman MJ, Yun TJ, Tarbell KV, Lesage S. The importance of dendritic cells in maintaining immune tolerance. *J Immunol*. 2017;198(6):2223-2231.

73. Vega-Ramos J, Roquilly A, Zhan Y, Young LJ, Mintern JD, Villadangos JA. Inflammation conditions mature dendritic cells to retain the capacity to present new antigens but with altered cytokine secretion function. *J Immunol*. 2014;193(8):3851-3859.

74. Biajoux V, Natt J, Freitas C, et al. Efficient plasma cell differentiation and trafficking require Cxcr4 desensitization. *Cell Rep*. 2016; 17(1):193-205.

75. Foulongne V, Sauvage V, Hebert C, et al. Human skin microbiota: high diversity of DNA viruses identified on the human skin by high throughput sequencing. *PLoS One*. 2012;7(6): e38499.

76. Byrd AL, Belkaid Y, Segre JA. The human skin microbiome. *Nat Rev Microbiol*. 2018;16(3): 143-155.

77. Ingle A, Ghim S, Joh J, Chepkoech I, Bennett Jenson A, Sundberg JP. Novel laboratory mouse papillomavirus (MusPV) infection. *Vet Pathol*. 2011;48(2):500-505.

78. Uberoi A, Yoshida S, Lambert PF. Development of an in vivo infection model to study Mouse papillomavirus-1 (MmuPV1). *J Virol Methods*. 2018;253:11-17.

79. Malissen B, Tamoutounour S, Henri S. The origins and functions of dendritic cells and macrophages in the skin. *Nat Rev Immunol*. 2014;14(6):417-428.

80. McDermott DH, Pastrana DV, Calvo KR, et al. Plerixafor for the treatment of WHIM syndrome. *N Engl J Med*. 2019;380(2):163-170.